HHS Public Access

Author manuscript

Curr Biol. Author manuscript; available in PMC 2021 December 07.

Published in final edited form as:

Curr Biol. 2020 December 07; 30(23): 4682–4692.e7. doi:10.1016/j.cub.2020.09.015.

Mouse higher visual areas provide both distributed and specialized contributions to visually guided behaviors

Miaomiao Jin, **Lindsey L. Glickfeld**

Department of Neurobiology, Duke University Medical Center, Durham, North Carolina 27710

Summary

Cortical parallel processing streams segregate many diverse features of a sensory scene. However, some features are distributed across streams, begging the question of whether and how such distributed representations contribute to perception. We determined the necessity of primary visual cortex (V1) and three key higher visual areas (LM, AL and PM) for perception of orientation and contrast, two features that are robustly encoded across all four areas. Suppressing V1, LM or AL decreased sensitivity for both orientation discrimination and contrast detection, consistent with a role for these areas in sensory perception. In comparison, suppressing PM selectively increased false alarm rates during contrast detection, without any effect on orientation discrimination. This effect was not retinotopically-specific, suggesting that suppression of PM altered sensory integration or the decision-making process rather than processing of local visual features. Thus, we find that distributed representations in the visual system can nonetheless support specialized perceptual roles for higher visual cortical areas.

In Brief:

Jin and Glickfeld use an optogenetic approach to interrogate the perceptual role of mouse higher-order areas. They find that LM and AL are required for perception of orientation and contrast, while PM has a distinct non-visual role. Thus, despite the broad representation of these features in the visual system, behavioral roles are specialized.

Graphical Abstract

Corresponding Author and Lead Contact: Lindsey Glickfeld, Department of Neurobiology, Duke Medical School, 311 Research Drive, BRB-401F, Durham, NC 27710, USA, glickfeld@neuro.duke.edu.

Author Contributions

M.J. and L.L.G. designed the experiments. M.J. collected and analyzed the electrophysiology and behavior data. L.L.G. collected and analyzed the calcium imaging data. M.J. and L.L.G wrote the manuscript.

Declaration of Interests

The authors declare no competing interests.

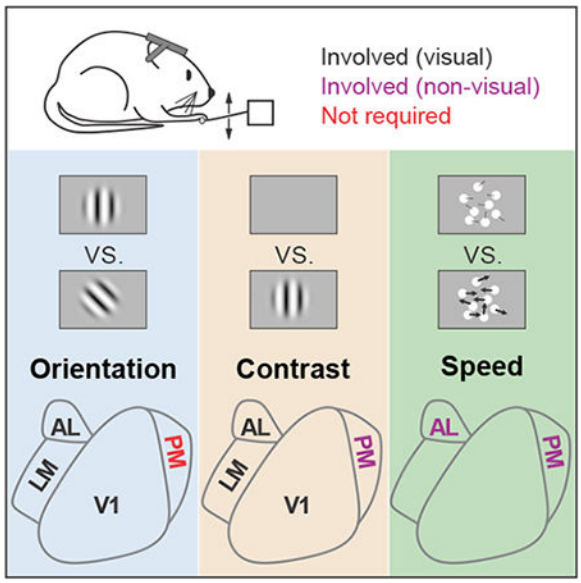

Keywords

mouse visual cortex; orientation; optogenetics; contrast; speed; psychophysics; sensory processing; decision-making; false alarm; d-prime

Introduction

Parallel processing is a fundamental organizing principle in sensory circuits [1–4]. The visual system is particularly parallelized with a large number of higher order cortical areas that each encode overlapping portions of the visual field [5–7]. This architecture is thought to enable functional specialization and read-out of receptive fields for behavior [8,9]. However, while there are some sensory stimulus properties that seem to be both functionally and perceptually localized to specific areas [10–12], there are also a number of examples of stimulus properties that have distributed representation across the visual system [13–15]. For instance, in the mouse visual system, the sensitivity of neurons to orientation and contrast is remarkably similar across higher order cortical areas [16–19]. These distributed representations beg the question of which areas are actually responsible for perception of these features.

One possibility is that the redundancy makes it such that no single higher area is necessary for the perception of distributed stimuli. This is particularly plausible in the mouse visual system where the primary visual cortex (V1) innervates at least nine higher visual areas (HVAs; [20]). Thus, this highly parallel organization could support a robust system in which the removal of any one area has little effect on the percept. In addition, V1 also encodes simple representations such as orientation and contrast and projects to a variety of subcortical areas such as the superior colliculus and pontine nuclei [21–23]. Thus, there is a direct route from sensory stimulus to action that could bypass higher cortical areas in the execution of simple behaviors.

Another possibility is that the entire distributed network is required to enable maximal sensitivity in perceptual performance. This might happen if the readout is monitoring the output of all areas, or if there is a hierarchical structure such that each area could act as a bottleneck [24,25].

There may also be intermediate conditions, potentially reflecting specialized anatomy or readout, in which only a subset of the distributed network contributes to perceptual sensitivity. Further, different areas may make distinct contributions to task performance. Indeed, HVAs that belong to the posterior parietal cortex seem to be more important for decision-making than sensory integration, despite receiving direct input from V1 [26–28]. Thus, careful dissection of multiple features of task performance, including hit, false alarm and lapse rates, is necessary to understand the function of each area in a distributed network.

We found evidence for both distributed and specialized contributions of three HVAs (LM: lateromedial; AL: anterolateral; PM: posteromedial) to perception of broadly represented features: orientation and contrast. While a distributed network including areas V1, AL and LM were required for perception of both orientation and contrast, the perceptual role of PM seems to be distinct from the lateral HVAs. PM was not required for the orientation discrimination task, despite task stimulus information being robustly encoded in all areas. The most reliable effect of suppressing PM was an increase in false alarm rate during the contrast detection task. This effect was independent of the alignment of the visual stimulus with the affected cortical representation, suggesting a more global role for PM in tasks involving the detection of weak signals on a noisy background. Consistent with this hypothesis, suppression of PM increased false alarm rates during a speed increment detection task in which the target-related neuronal activity is prone to be confused with spontaneous fluctuations in the population. Thus, our results provide evidence that distributed representations are neither completely robust to perturbation of single areas nor homogenously supported by all areas, thereby revealing clear functional specialization in the visual system.

Results

Rapid and reversible suppression of mouse visual cortical areas

To determine the involvement of visual cortical areas in perceptual decision-making, we suppressed neuronal activity within specific HVAs by expressing excitatory opsins (Channelrhodpsin-2 or Chronos (ChR)) in GABAergic interneurons [29–31]. We targeted conditional viral expression of ChR to either V1 or an HVA (LM, AL or PM; Figures 1A and S1) in lines which express Cre recombinase in inhibitory interneurons (PV::Cre, n=10 mice; GAD::Cre, n=2 mice).

To validate the temporal and spatial resolution, we made extracellular single unit recordings with multi-pronged electrodes that spanned up to 1.2 mm from the center of the injection site. The majority of cells near the injection site were significantly suppressed (58/82 cells; Figure 1B, **right**). Suppression was stable for the four second light stimulation (p=0.81, Kruskal-Wallis test across time bins (bin size: 100 ms), DF=36, n=58 cells, 16 experiments, 12 mice), and did not drive significant rebound excitation when the light was extinguished

(first 200 ms after LED offset vs. baseline activity: p=0.40, Wilcoxon signed rank test). Thus, there is stable suppression of neuronal activity for the full duration of each behavioral trial and independent control across trials.

We also found that spatial spread of suppression enables reasonably independent control of V1 and the HVAs. The degree of suppression rapidly decayed with distance from the injection site with a space constant of 464 μm (95% CI: [354 594 μm]; $p<10^{-17}$, Kruskal-Wallis test, n=301 cells, Figure 1C). We used this space constant to estimate the degree to which suppression within any one visual area might spread to other areas. First, we measured the relative position and size of the region within V1 and each HVA that would be activated by the visual stimulus used in the behavioral tasks with intrinsic autofluorescence imaging (n=15 mice). Then, we determined the percentage of suppression of each area given its distance from the targeted area and the space constant (Figure 1D). This revealed that suppression targeted to V1 was well-restricted within V1 (area coverage: V1:94±2%; all other areas: 0%; Figure 1E), and suppression targeted to any HVA did not spread to V1. However, suppression targeted to the HVAs was not completely restricted to that HVA. For instance, while AL and LM were largely independent, there was ~20% overlap in each direction (target AL, 21±5% LM affected; target LM, 18±5% AL affected), and AM and PM share ~85% overlap (target: PM, 86±6% AM affected; target AM, 84±5% PM affected). Thus, this viral approach enables reasonable independent control of V1, LM and AL. To further improve the independent suppression of PM, we targeted our viral injection a few hundred microns posterior from the retinotopic center of PM, to avoid strong suppression of AM, but still suppress PM.

In some experiments, we also used a transgenic line to express ChR in GABAergic interneurons (VGAT-ChR2; n=2 mice; [31]). Neurons recorded in these mice exhibited clear rebound excitation after light offset ($p<10^{-5}$, Wilcoxon signed rank test; Figure S2A–B). The degree of suppression was weaker (p=0.001, Wilcoxon rank sum test) and spread further away from the light center as compared to the viral approach (interaction between method and cortical distance: $p<10^{-6}$, two-way ANOVA, Figure S2C–E). Therefore, we used the viral approach for the majority of experiments testing the perceptual effects of area suppression (PV::Cre- n=25 mice; GAD::Cre- n=1 mouse; VGAT-ChR2- n=5 mice). Nonetheless, the behavioral results were comparable across approaches (Figure S3).

Role of mouse visual cortical areas in a go/no-go orientation discrimination task

Stimulus orientation is a fundamental feature that is robustly encoded in the visual system of most species, including mouse V1 and the HVAs [18,19]. While V1 is known to be required for tasks involving discrimination of stimulus orientation [30,32–34], it is not known which, if any, higher visual areas are necessary for the perception of this distributed representation.

Therefore, we trained mice to perform a go/no-go orientation discrimination task (Figure 2A, [33,34]). In this task, the mice press a lever to initiate the trial and trigger the repeated presentation of a 100 ms, static, vertically-oriented, sinusoidal gabor (2-10 distractors; 250-750 ms inter-stimulus interval (ISI)) followed by the presentation of a target orientation (8-90° counter-clockwise difference from the distractor). The mice must release the lever within a brief reaction window after target onset to indicate discrimination of the target and

receive water reward. Release of the lever within 200-550 ms after target onset was counted as a “hit”, while failure to release during this window was counted as a “miss”. We thus quantified hit rate as a function of target orientation to construct a psychometric function to measure discrimination threshold (Figure 2B–E, left). Similarly, if animals released the lever within the same window following a distractor presentation, it was categorized as a false alarm (FA), and otherwise a correct reject (CR), giving us a measure of FA rate (Figure 2B–E, right). Notably, we chose stimulus properties including size (30° diameter), position (30-40° azimuth, 0-10° elevation), and spatial frequency (0.1 cycles/degree) that effectively drive neurons in V1 and each of the HVAs [7,16,19].

To determine the role of visual cortical areas on this task, we suppressed activity in the cortical hemisphere contralateral to the visual stimulus on interleaved trials. Suppression was initiated at the time of trial onset and terminated after the mouse released the lever or the reaction time expired. Notably, we used relatively low light powers to avoid heating the brain or impairing the animals on the easiest trials (i.e. 90° targets), so that we could avoid confounds associated with changes in task engagement.

In control conditions, mice had an average threshold of 20±1°, FA rate of 0.10±0.01 and d’ of 1.4± 0.1 (at near threshold orientation 22.5°; n=18 mice). Suppressing V1, LM and AL significantly increased the animals’ orientation discrimination threshold (V1: p=0.002, n=6 mice; LM: $p<10^{-3}$, n=7; AL: $p<10^{-3}$, n=7; paired t-test; Figure 2F,L and Data S1) and decreased the FA rate (V1: $p<10^{-3}$; LM: p=0.004; AL: p=0.001; paired t-test; Figure 2G,L and Data S1). The large decrease in both hit and FA rate resulted in a significant increase in bias in all three areas, consistent with a coincident decrease in both signal and noise (V1: $p<10^{-3}$; LM: $p<10^{-3}$; AL: $p<10^{-3}$; Figure S4A). The magnitude of these effects was equivalent across all three areas (threshold: p=0.65; FA: p=0.22; bias: p=0.33; one-way ANOVA across areas), suggesting that V1, LM and AL are similarly involved in orientation discrimination. However, when we suppressed area PM, we did not observe any significant difference in discrimination threshold (p=0.90, n=5 mice), FA rate (p=0.92) or bias (p=0.95), suggesting a lack of role for PM.

This lack of effect with PM suppression cannot be explained by the efficacy of suppression since we observed similar degree of effect of ChR activation in PM as in V1 and AL, and only a slightly stronger effect in LM (Kruskal-Wallis test (p=0.007) with post-hoc Dunn’s test comparing to PM (n=20 cells): V1: p=0.92, n=54; AL: p=0.09, n=28; LM: p=0.03, n=6; Figure 3A–B). The lack of effect of suppression of PM on this task was also not clearly explained by differences in visual response properties across areas. There was a significantly smaller fraction of neurons in PM driven by task stimuli (V1: 272/357, 0.76; LM: 112/150, 0.75; AL: 135/172, 0.78; PM: 108/191, 0.57; $p<10^{-5}$, df=3; chi-square test), and visually-driven cells in PM had significantly lower firing rates than AL in response to the early stimuli ($Stim_{1st}$: Median firing rate with 25th and 75th percentile- V1: 5.8 [3.6 9.9] Hz, LM: 5.4 [2.9 9.8] Hz, AL: 6.5 [3.2 12.4] Hz, PM: 4.8 [3.0 8.0] Hz; all comparisons with PM: V1- p=0.11, 17.2% lower; LM- p=0.66, 11.1%; AL- p=0.05, 26.1%; Kruskal-Wallis test (p=0.05) with post-hoc Dunn’s test; Figure 3C–D) and also lower than AL and V1 in response to late stimuli ($Stim_{4th\text{-}5th}$- V1: 3.5 [1.8 6.2] Hz, LM: 2.3 [1.0 5.4] Hz, AL: 3.2 [1.5 6.8] Hz, PM: 2.1 [1.1 4.4] Hz; all comparisons with PM: V1- p=0.001, 40.0% lower; LM- p=0.97, 8.7%;

AL- p=0.02, 34.3%; Kruskal-Wallis test ($p<10^{-3}$) with post-hoc Dunn's test). However, neurons in all areas were similarly orientation tuned (p=0.23; one-way ANOVA; Figure 3E) and had similar signal-to-noise ratio (SNR, mean/std) at their preferred orientation (p=0.18; one-way ANOVA; Figure 3F). Thus, despite there being fewer neurons with robust visual responses in PM, there was nonetheless a large population of neurons in PM with task-relevant stimulus information that could be used for discriminating orientation.

Suppressing V1, LM and AL significantly decreased sensitivity (d' for 22.5° target: V1: p=0.02; LM: p=0.004; AL: $p<10^{-3}$; Figure 2H; [35]), consistent with a sensory role for these areas in orientation discrimination. Indeed, when we moved the visual stimulus presentation to the ipsilateral field of view (relative to the suppression site; Data S2), all effects of cortical suppression were abolished (all effects on threshold, FA rate, sensitivity and bias- p>0.1; Figure 2I–K and S4A). This suggests that the effects of suppression of V1, LM and AL on performance of orientation discrimination are specific and restricted to the silenced retinotopic positions.

Non-visual aspects of task performance, such as task engagement and target expectation, were not affected by suppression of the visual cortical areas (Figure S5). First, we found no change in the lapse rate (1-hit rate at the easiest target) when suppressing V1 (p=0.33) or PM (p=0.40). We did observe a small but significant increase in lapse rate with suppression of LM (p=0.04) and AL (p=0.005, paired t-test; Figure S5A), however there was a strong correlation between the change in lapse rate and the change in threshold and FA rate, suggesting that this is due to a visual impairment rather than task engagement (threshold: r=0.54, p=0.006; FA rate: r=−0.36, p=0.08). Secondly, target expectation also changed over the course of a trial, such that animals reliably had lower thresholds ($p<10^{-5}$, n=15 mice, one-way ANOVA) and higher FA rates ($p<10^{-6}$) late in the trial, due to an increase in the probability of target occurrence with the hold time. Suppressing visual areas did not affect the dependence of either threshold or FA rate on trial length (interaction between area suppression and trial length: all effects on threshold and FA rate- p>0.5; two-way ANOVA; Figure S5B–C), suggesting a lack of a role for these areas in expectation.

In summary, we found that V1 and higher visual areas LM and AL, but not PM were required for this orientation discrimination task. The fact that the effects of V1, LM and AL suppression had no effect on non-visual aspects of the task and were specific to the affected visual field supports a mainly perceptual role of these areas.

Role of mouse visual cortical areas in a go/no-go contrast detection task

Stimulus contrast, like orientation, robustly modulates neuronal activity across all visual areas [16,17]. To determine which, if any of the three HVAs is required for perception of this broadly represented stimulus feature, we next trained mice on a go/no-go contrast detection task ([30,36]; Figure 4A).

As in the orientation discrimination task, in the contrast detection task the mice must press the lever to initiate each trial and release the lever to report detection of a contrasted target grating (0°, 100 ms duration, contrast range: 4%-100%; Figure 4A). We quantified hit rate by calculating percentage of target presentations in which the mouse released within the

reaction time window (200-550 ms) after target onset (Figure 4B, **left**). We also calculated FA rate by assessing the percentage of releases within a similar window before target appearance (Figure 4B, **right**).

On control trials, mice had an average threshold of 9.6±0.7% contrast, FA rate of 0.06±0.005 and d' of 1.6±0.1 (at near threshold contrast 10%; n=19 mice). We found that suppressing V1, LM and AL significantly increased the contrast detection threshold (V1: p=0.006, n=6 mice; LM: p=0.02, n=7; AL: p=0.004, n=6; paired t-test; Figure 4F, 4L **top and** Data S3), while suppression of PM slightly, but not significantly, increased the threshold (p=0.08, n=12), resulting in a significantly weaker effect of suppression of PM than other areas (PM vs. V1: $p<10^{-4}$; PM vs. LM/AL: p=0.02; one-way ANOVA ($p<10^{-4}$) with post hoc Tukey HSD test).

Instead, suppressing PM had the surprising effect of increasing the FA rate (p=0.01, paired t-test; Figure 4G **and** 4L **bottom**). Notably, this is unlike V1, where suppression decreased FA rate (p=0.02), and also unlike AL and LM, where suppression had no reliable effect (LM: p=0.94; AL: p=0.71). These changes in hit and FA rate led to an increase in bias in V1, LM and AL (c for 10% contrast- V1: p=0.006; LM: p=0.006; AL p=0.005; PM=0.57; paired t-test; Figure S4B) and a consistent decrease in sensitivity across all areas (d' for 10% contrast- V1: p=0.009; LM: $p<10^{-4}$; AL: p=0.02; PM: $p<10^{-3}$; Figure 4H), suggesting a sensory role for each area. However, while moving the stimulus to the ipsilateral field abolished the increase in threshold in V1, LM and AL (V1: p=0.99, n=3 mice; LM: p=0.24, n=4; AL: p=0.03, n=4; paired t-test; Figure 4I **and** Data S4), suppression of PM still trended towards increasing the FA rate (p=0.09, Figure 4J). Notably, there was no significant difference between contralateral and ipsilateral conditions for mice that had both conditions (p=0.39, n=5 mice, paired t-test), suggesting that the effect of PM on FA rate is not retinotopically-specific. The effect of suppression of PM also did not depend on the genotype used for optogenetic suppression (VGAT/GAD::Cre (n=4) vs PV::Cre (n=8): p=0.27; Figure S3B), suggesting that the increase in FA rate is not an artifact of the method of suppression.

Thus, we found that V1, LM and AL were required for both orientation discrimination and contrast detection. In comparison, while PM was not required for discriminating orientations, it was involved in performance of the contrast detection task. Namely, while we found suppression of PM weakly increased detection thresholds, the more robust effect was a reliable increase in FA rate, which was independent of visual stimulus input.

Role of mouse visual areas in a go/no-go speed increment detection task

To address why suppression of PM increased FA rate in the contrast detection task but not in the orientation discrimination task, we considered what different neuronal computations might be important for the two tasks. Increases in stimulus contrast typically drive monotonic increases in firing rate in the four areas [16]. Thus, to detect low contrast stimuli, the decision-making circuit has to identify a small, transient increase in population activity. A system tuned to detect such events will be extremely sensitive to the level of background noise, such that spontaneous fluctuations in neuronal firing might be perceived as a target. Further, the temporal structure of the task, in which targets can appear up to 4 seconds after

trial initiation, further exacerbates the potential influence of noisy background activity as there is no temporal context to aid in distinguishing signal from noise. In comparison, during the orientation discrimination task, the high contrast orientation presentation drives a strong signal, with defined timing, that may be less sensitive to small background fluctuations. Thus, we considered the possibility that suppressing PM might alter the frequency or amplitude of such noisy background fluctuations leading to an increase in FA rate during the contrast detection task.

To determine if PM might have similar effects on FA rate during a task that is structurally and computationally similar to the contrast detection task, we developed a new speed increment detection. In this task, the mouse must detect a speed increment of a field of randomly moving dots with 0% coherence in stimulus direction (Figure 5A). As in the contrast detection task, animals initiated the task by pressing the lever and released the lever within a reaction time window to report a speed increment of the moving dots (0% coherence, baseline speed: 0.5 deg/s, speed increment: 0.94-30 deg/s).

Since neurons in AL and PM have distinct speed preference profiles in response to drifting gratings [18,19,37–40], and therefore may be important for speed change detection, we focused on the role of these two areas. To understand how neurons in these areas integrate task stimuli, we used two-photon calcium imaging to measure responses to speed increments in passively viewing mice transgenically expressing GCaMP6. In AL and PM, a similar proportion of neurons were (AL: 669/747, 0.90; PM: 516/564, 0.91; p=0.79), though significantly more neurons in AL were tuned to speed (AL: 337/669, 0.50; PM: 196/516, 0.38, p=0.008). We found that population neuronal response incremented monotonically with speed in both areas (Figure 5B–C). Moreover, the majority of tuned neurons in each area preferred the fastest speed (AL: 229/337, 0.68; PM: 143/196, 0.73; p=0.61; p=0.61; Figure 5D) and were well-fit by the Naka-Rushton function (AL: 259/337 0.77, PM: 148/196, 0.76; p=0.9), a monotonically incrementing function often used to approximate contrast-response functions. Thus, both AL and PM have neuronal activity that can be used to detect speed increments, and this feature is encoded similarly to contrast (i.e. with a monotonic increase in population activity) in both areas.

To determine the effect of suppressing AL and PM on task performance, we used the same approach as in the contrast detection task to calculate hit rate, detection threshold and FA rate on the speed increment detection task (Figures 5E–F **and** Data S5). In control trials, mice had an average threshold of 1.9±0.2 deg/s, FA rate of 0.12±0.02 and d’ of 1.3±0.1 (at near threshold speed 2 deg/s; n=5 mice). While AL suppression did not have consistent effects on speed increment detection threshold (p=0.42, n=5 mice, paired t-test; Figure 5G **and** Data S5A) and FA rate (p=0.13, Figure 5H), PM suppression consistently decreased detection threshold (p=0.01, n=5 mice) and increased FA rate (p=0.01). In this case, there was a decrease in bias (p=0.005; Figure S4C) and no change in sensitivity with PM suppression (p=0.17; Figure 5I). Consistent with this lack of a sensory role for PM, these effects were maintained when we presented the visual stimulus ipsilateral to the suppression site (PM- threshold: p=0.05; FA rate: p=0.05; bias: p=0.04; n=2 mice; Figure 5J–L, S4C **and** Data S5B). Interestingly, moving the stimulus to the ipsilateral field also revealed a decrease in threshold, an increase in FA rate, and a decrease in bias when suppressing AL (AL-

threshold: p=0.02; FA rate: p=0.03; bias: p=0.01; n=3 mice), suggesting that there may be some competing effects of suppressing AL during speed increment detection.

In summary, we found that suppression of PM consistently increased FA rate on both the contrast and speed increment detection task independent of effects on sensory processing. This suggests that PM may have a role in regulation of sensory integration or the decision-making process, for instance through altering noise levels in the visual system.

Discussion

We found functional specialization of mouse HVAs in perception of broadly represented visual features, such as orientation and contrast. While lateral HVAs (LM and AL) contribute to perception of both orientation and contrast, a medial HVA (PM) was not required for discriminating orientations and had a much weaker contribution to contrast detection than lateral HVAs. Notably, suppression of PM consistently increased FA rate in both contrast and speed increment detection tasks independent of visual processing, suggesting that rather than processing local visual features, PM might directly affect sensory integration or the decision-making process.

One major finding is that mouse lateral HVAs (LM and AL) are required for perception of simple visual features such as contrast and orientation. Suppression of these areas significantly increases thresholds and decreases sensitivity, and these effects are dependent on the retinotopic alignment of the suppressed neuronal population with the visual stimulus, consistent with a sensory role for these areas. Notably, there was also a robust decrease in FA rate, leading to an increase in bias, likely reflective of a decrease in both the signal and the noise [33]. This argues that even these relatively simple perceptual tasks require the routing of visual signals through distributed HVAs, and do not rely solely on a pathway from V1 directly to decision-making areas. We do not think the effects of LM and AL on behavior are the result of “off-target” effects of the removal of excitation to their targets [41,42]. For one, while LM and AL both send excitatory projections back to V1 [43], suppression of these areas do not silence V1 [44,45], and in some cases actually increase excitability due to a decrease in surround suppression [46]. Further, that suppression of LM and AL have a similar magnitude effect as suppression of V1 suggests that these areas lie downstream of V1 in the perceptual pathway. However, we cannot rule out that LM and AL have indirect contributions to perception by modulating processing in other targets such as the superior colliculus and striatum [41,47,48].

The comparable effects of LM and AL on these behaviors also suggests that both are important for the computation. Given that suppression of either LM or AL only weakly influenced activity in the neighboring area, one would expect asymmetric effects on behavior if only one was important. This distributed contribution of lateral HVAs to perception is notable given the distinct stimulus preferences of these areas [18,19], and might reflect the underlying functional organization of the mouse visual system. One possibility is that these areas might have redundant roles, with the intact area partially compensating for the silenced one. However, the comparable effect of suppressing each area argues against the redundancy of the circuits. It is more consistent with the information

being routed from V1➔LM➔AL [25,49,50]. Alternatively, the decoder might need to integrate the information encoded in both areas in order to achieve maximum accuracy, such that impairing either area affects performance.

Another important finding is the existence of functional specialization for perception of features. In comparison to V1, LM and AL, suppression of PM had no effect on performance of the orientation discrimination task. This is not a trivial result as neurons in PM are responsive to task stimuli, orientation tuned, and suppressed by activation of inhibitory interneurons. Moreover, studies using decoding analysis to classify stimulus orientation from population activity found performance was either similar between PM, LM and AL [51], or only slightly higher in AL than in LM and PM [17,52]. Thus, our data suggest that there is information present in PM that is not used to perform this orientation discrimination task. Further, given the strong responsivity of neurons in both AL and PM to speed increments, the lack of impairment on the speed task is also notable. These results add to an accumulating literature suggesting that encoding of task-related information does not always guarantee a causal relationship of that area in behavior [28,53–56]. There are many potential explanations for this disconnect between encoding and decision-making. One possibility is that PM does use these signals for behavior, but only under specific task or environmental contexts. Second, it is possible that while we chose stimulus features that effectively activate PM (high spatial frequency, low temporal frequency [18,19]), we did not explore the stimulus space in which it is behaviorally engaged. Finally, it is possible that the orientation and speed information found in PM is simply inherited along with other visual signals that are used for behavior.

The third key finding is that roles of HVAs in perceptual decision-making may not be purely sensory. While there was no effect of PM on the orientation task, suppression of PM did cause a small decrease in sensitivity on the contrast detection task, in part due to an increase in FA rate. This increase in FA rate was independent of the alignment of the suppressed neurons with the visual stimulus, suggesting that the effect is not sensory. We do not think that this can be explained by a direct effect on motor output, because there is no increase in FA rate on the orientation discrimination task. Instead, we propose that decreasing activity in PM might act to disinhibit some target area, thereby leading to an increase in the fluctuation of background activity. Such an increase in noise might make the downstream decoder more likely to inappropriately pass threshold, especially on a task where the circuit is optimized to detect small increases in activity. If this noise impacts a sensory area, it might even drive a fictive percept, like a phosphene. Notably, we would still consider such an event the result of increased noise, as it is not driven by task-related sensory input.

The effects of PM on FA rate may act through a variety of sensory or decision-making areas. PM provides excitatory input to V1, the other HVAs, superior colliculus, higher order thalamic nuclei, and the cingulate cortex, among others [47,57,58]. These pathways can often have a net inhibitory effect through the recruitment of local inhibition [46,59,60]. Moreover, a recent study suggests suppression of the lateral posterior (LP) nucleus of thalamus could increase the excitability in V1 resulting in an increase FA rate in a visual discrimination task [61]. Thus, PM suppression might act through this LP➔V1 circuit. Alternatively, the effects of PM may reflect its feedforward influence on decision-making

areas, such as the colliculus or striatum, rather than the feedback influence on sensory integration. Indeed, suppression of PM during the speed change detection task does decrease bias, potentially consistent with a shift in decision criterion. However, the complicated interaction of sensory and cognitive contributions to the measure of bias prevent a clear delineation of where in the sensory processing pathway PM might be acting [33].

Notably, the effect of suppression of PM on FA rate may not be unique. While suppression of LM and AL do not drive an increase in FA rate during the contrast detection task, nor do they drive a decrease in FA rate as they did in the orientation discrimination task. Thus, this lack of a change may reflect the competition between two mechanisms. Indeed, in the speed increment detection task, we observed an increase in FA and hit rate when suppressing ipsilateral AL without a decrease in FA and hit rate when suppressing contralateral AL. This suggests that the retinotopic-specific visual effects of suppressing an HVA might be obscured by the global non-specific effects. Conversely, the visual effects of suppressing PM during the contrast detection task may be masked to some degree by the changes in FA rate, resulting in the net zero change in bias.

In summary, although orientation and contrast are broadly represented throughout the mouse visual system, the circuits required for perception of these features are not similarly distributed. While some areas, like LM and AL are clearly required for discriminating orientations and detecting contrast, the role of PM in these tasks is more complex. This difference between the medial and lateral HVAs begs the question of what might support the difference in the readout of information. One possibility is the difference in downstream connectivity [58]; another possibility is that the outputs of these areas are differentially integrated by their targets to drive a decision [34,62]. Understanding how each area performs its discrete role will help us understand the computations that link sensation and action.

STAR Methods

RESOURCE AVAILABILITY

Lead Contact.—Requests for information and resources should be directed to the Lead Contact: Lindsey L. Glickfeld (glickfeld@neuro.duke.edu).

Materials Availability.—This study did not generate new unique reagents.

Data and Code Availability.—The primary behavioral data are provided on Mendeley Data (https://data.mendeley.com/datasets/923tpcfrsg/1). In addition, the performance of each individual mouse in orientation discrimination, contrast and speed increment detection tasks are provided in Data S1–S5. Due to the large size of the data files, the primary electrophysiological and imaging datasets are available upon request from the Lead Contact. The analysis code supporting this manuscript are available on Github (https://github.com/Glickfeld-And-Hull-Laboratories/ImagingCode-Glickfeld-Hull/tree/master/lindsey/Manuscripts/JinGlickfeld_CurrentBiology).

EXPERIMENTAL MODELS AND SUBJECT DETAILS

Animals.—All animal procedures conformed to standards set forth by the Public Health Service policy of the NIH, and were approved by the IACUC at Duke University. 59 mice (both sexes; 3-30 months old; singly and group housed (1-4 in a cage) under a regular 12-h light/dark cycle; C57/B6J (Jackson Labs #000664) was the primary background with up to 50% CBA/CaJ (Jackson Labs #000654)) were used in this study. *Pvalb-cre (tml(cre)Arbr,* Jackson Labs #008069; n=39; PV::Cre), *VGAT-ChR2-EYFP (Slc32a1-COP4*H134R/EYFP,* Jackson Labs #014548; n=7), *Gad2-IRES-cre (Gad2tm2(cre)Zjh,* Jackson Labs #010802; n = 4; GAD::Cre), Emx1-IRES-Cre *(tm1(cre)Krj,* Jackson Labs # 005628; n=2) and Wild-type (n=1) were used for *in vivo* extracellular electrophysiology (n= 27), and behavior (n=31) experiments (note five mice were used in both behavior and electrophysiology). For calcium imaging experiments, six mice transgenically expressing GCaMP6 were used (Ai93 [*tm93.1(tetO-GCaMP6f)Hze;* Jackson Labs #024103] were crossed to Emx1-IRES-Cre and CaMK2a-tTA (Jackson Labs #003010; n=1) and Ai162 [*tm162.1(tetO-GCaMP6s,CAG-tTA2)Hze;* Jackson Labs #031562] were crossed to Slc17a7-IRES2-Cre-D [*tm1.1(Cre)Hze;* Jackson Labs #023527; n=5).

METHODS DETAILS

Cranial window implant.—Animals were implanted with a titanium headpost and 5 mm cranial window as previously described [63]. Briefly, dexamethasone (3.2 mg/kg, s.c.) and Meloxicam (2.5 mg/kg, s.c.) were administered at least 2 h before surgery. Animals were anesthetized with ketamine (200 mg/kg, i.p.), xylazine (30 mg/kg, i.p.) and isoflurane (1.2-2% in 100% O_2). Using aseptic technique, a headpost was secured using cyanoacrylate glue and C&B Metabond (Parkell), and a 5 mm craniotomy was made over the left hemisphere (center: 2.8 mm lateral, 0.5 mm anterior to lambda) allowing implantation of a glass window (an 8-mm coverslip bonded to two 5-mm coverslips (Warner no. 1) with refractive index-matched adhesive (Norland no. 71)) using Metabond.

The mice were allowed to recover for one week before habituation to head restraint. Habituation to head restraint increased in duration from 15 min to >2 h over 1-2 weeks. During habituation, imaging and electrophysiology sessions, mice were head restrained while either allowed to freely run on a circular disc (InnoWheel, VWR) or rest in a plastic tube.

Retinotopic mapping.—Retinotopic maps were generated from GCaMP fluorescence, intrinsic autofluorescence or cortical reflectance (for *VGAT-ChR2-EYFP* mice). For intrinsic autofluorescence (Figure 1A and S1), the brain was illuminated with blue light (473 nm LED (Thorlabs) or a white light source (EXFO) with a 462 ± 15 nm band pass filter (Edmund Optics)), and emitted light was measured through a green and red filter (500 nm longpass). For GCaMP imaging, the same excitation light was used, but emitted light was measured through a 520 ± 18 nm band pass filter. For cortical reflectance (Figure S2A), the brain was illuminated with orange light (530 nm LED (Thorlabs)), and all of the reflected light was collected. For all conditions, images were collected using a CCD camera (Rolera EMC-2, Qimaging) at 2 Hz through a 5x air immersion objective (0.14 numerical aperture (NA), Mitutoyo), using Micromanager acquisition software (NIH). Images were analyzed in

ImageJ (NIH) to measure changes in fluorescence (dF/F; with F being the average of all frames) to identify V1 and the HVAs.

To robustly identify the visual areas, we used a two-stage approach for retinotopic mapping (Figure S1). First, the monitor was positioned at 45° relative to the body axis, and stimuli were presented at 3 positions (Elevation (El): 10 deg, Azimuth (Az): −10, 10 and 30 deg, 40° sinusoidal gratings, drifting at 2 Hz, 10 s duration, 10 s inter-trial interval) to activate locations in the contralateral visual field (Figure S1A). This allowed us to identify sites of retinotopic reversals to define area identity and boundaries [7,16,20]. Next, we positioned the monitor at 0° relative to the body axis, and stimuli were presented at the location used during the behavioral task (El: 10, Az: 30-40 deg, green in Figure S1B). We used these maps to measure the distance between areas (Figure 1D–E) and target our viral injections to the retinotopic location activated by the task stimulus. Vascular landmarks were used to identify sites for targeted viral injections, electrophysiology, and calcium imaging. In some cases, PM and AM were not entirely separable in the location of the behavior task. But we could always easily define their boundaries by using more lateral stimuli positions (Figure S1A). For calcium imaging experiments, only the 45° monitor position was used, and stimuli were presented at 9 positions (Elevation (El): 15, 0 −15 deg, Azimuth (Az): −30, 0 and 30 deg, 30° sinusoidal gratings, drifting at 2 Hz, 5 s duration, 5 s inter-trial interval) for clear separation of areas.

Viral injection.—We targeted V1, or AL and PM, or LM and PM in PV::Cre or GAD::Cre mice for viral expression of Channelrhodopsin2 (ChR2) or Chronos. Dexamethasone (3.2 mg/kg, s.c.) was administered at least 2 h before surgery and animals were anesthetized with isoflurane (1.2-2% in 100% O_2). The coverslip was sterilized with 70% ethanol and the cranial window removed. A glass micropipette was filled with virus (AAV5.EF1.dFloxed.hChR2.YFP (titer: 3.74e12 GC/ml; UPenn CS0384), AAV9.CAGGS.FLEX.ChR2.tdTomato (titer: 2.44e12 GC/ml; Addgene 18917) or AAV1.Syn.FLEX.Chronos.GFP (titer: 4.80e12 GC/ml; Addgene 62722)), mounted on a Hamilton syringe, and lowered into the brain. 30-50 nL of virus (30 nl for HVAs; 50 nl for V1) were injected at 250 and 500 pm below the pia (30 nL/min); the pipette was left in the brain for an additional 10 minutes to allow the virus to infuse into the tissue. Following injection, a new coverslip was sealed in place, and for behavioral experiments, an optical fiber (400 pm diameter; Doric Lenses) was attached to the cranial window above the injection site. Optogenetic behavioral experiments and electrophysiology experiments were conducted at least two weeks following injection to allow for sufficient expression. On average, the expression covered 0.77±0.28, 0.38±0.09, 0.52±0.12, and 0.33±0.03 mm^2 for V1 (n=5), LM (n=7), AL (n=12) and PM (n=15) respectively (p=0.07, one-way ANOVA across areas).

Visual stimulation.—Visual stimuli were presented either on a 144-Hz (Asus) or 120-Hz (Samsung) LCD monitor for electrophysiology and behavior experiments, respectively. Monitors were calibrated with an i1 Display Pro (X-rite) for mean luminance at 50 cd/m^2 and positioned 21 cm from the eye. The stimulus presentation protocols in behavior, electrophysiology and imaging experiments are described in each section.

Behavioral task.—Animals were water scheduled and trained to discriminate the orientation of visual stimuli, or detect the appearance of a visual stimulus with varying contrast, or detect the increment of speed of the moving dots by manipulating a lever. The behavior training and testing occurred during the light hours of their daily cycle. All behavioral control and stimulus presentation used MWorks (https://mworks.github.io/), and custom software in MATLAB (MathWorks).

The go/no-go orientation discrimination task was trained and performed as previously described [34] (Data S1–2). Briefly, each trial was initiated when the ITI (3s) had elapsed and the mouse had pressed the lever. Trial start triggered the presentation of a series of 100 ms static sinusoidal, gabor patches (diameter: 30°, spatial frequency (SF): 0.1 cycle/deg, contrast: 100%, positioned at an eccentricity of 30° - 40° in azimuth and 0° - 10° in elevation) followed by a target orientation of the same parameters but of a different orientation. The spatial frequency value was chosen to ensure the task stimuli drive all HVAs equally well (Figure 3C–D). The target orientation occurred with a variable delay (flat distribution) after at least two distractor presentations (up to 10 distractors). Following each target, additional distractors were presented until the mouse either released the lever or the reaction time expired. Within each trial, each stimulus presentation (distractor or target) was separated by a mean-luminance ISI (either constant at 250 ms, or randomized between 250, 500 and 750 ms). Each trial had the possibility of having a target presentation, if the mouse held the lever through the all of the preceding distractor presentations. Mice received water reward only if they released the lever within 100-650 ms (sometimes extended to 1000 ms) after a target occurred. If mice released the lever before reaction time began (early release) or failed to release the lever by the time the reaction time expired (miss), the trial would be aborted and additional time (2-4s) would be added to the ITI. Notably, this reaction window is different than the window used to analyze hit and FA rates (200-550 ms). The analysis window was chosen to make the reaction window for each stimulus presentation independent so that the hit/FA could be assigned to a specific presentation. Indeed, the majority of lever releases occur during this analysis window [34]; however, during the task performance we rewarded releases in a slightly broader window to achieve more stable behavior.

The go/no-go contrast detection task was trained and performed as previously described [36] (Data S3–4). Briefly, as in the orientation discrimination task, each trial was initiated when the ITI (3s) had elapsed and the mouse had pressed the lever. Following a variable period (from 700-3500 ms), a static sinusoidal target grating (diameter: 30°; SF: 0.1 cycle/deg; azimuth of 30° - 40°; elevation of 0° - 10°) of a variable contrast (range: 4%−100% contrast) was presented. Delays after errors were also added to discourage lapses and early releases.

For the go/no-go speed increment detection task (Data S5), we first trained mice to detect an increase in speed of the random dot kinetogram (speed increase from stationary to 30 deg/s; full-field; 100% coherence in nasal to temporal direction; dot density: 0.025; dot size: 3 deg) that started at the end of the required hold time (400 ms). Once the animals started to respond to the change of speed by releasing the lever, we gradually made the task harder by: 1) decreasing the dots coherence to 0%; 2) increasing the random delay (final max value: 4 s) between the lever press and speed increment; 3) shrinking the field size and moving it to

more eccentric positions (30° in diameter; azimuth of 35°; elevation of 10°); 4) increasing baseline speed from 0 to 0.5 deg/s; and 5) introducing hard target speeds (difference from the baseline speed: 0.94-30 deg/s) to probe speed increment detection threshold. Delays after errors were also added to discourage lapses and early releases.

We delivered blue light to the brain though an optic fiber from a 473 nm LED (Thorlabs) or a 450 nm laser (Optoengine) and calibrated the total light intensity out of the fiber. For all behavior tasks, the light was delivered on 50% of trials (randomized with control trials) for the entire duration of the trial and terminated after the animal either released the lever or the reaction window expired. A black cap was used to block the blue light to minimize the chance of animal detecting the light delivery. The light power was chosen independently for each mouse such that there was a minimal effect on hit rate on the easiest trials, while potentially still affecting behavior on trials near threshold. This meant that there could be variability in the light power used across mice, as well as within mice across tasks (Table 1). In particular, this resulted in the use of higher light powers when suppressing PM to maximize the chance of seeing an effect. Note that for behavior tests using VGAT-ChR2 transgenic mouse line, the light power never exceeded 0.4 mW to minimize spatial spread of cortical suppression (Figure S3, [31]).

For all tasks, trial difficulty was adjusted independently for each mouse by changing the exponent of the log spacing of target orientation, contrast or speed. This allowed us to sample multiple points along the steepest part of the psychometric function to best estimate the discrimination/detection threshold, despite there being a range of thresholds across our cohort of mice. In the case that optogenetic suppression significantly increased the threshold, we also adjusted the set of targets presented on suppression trials in order to accurately measure thresholds in these conditions as well.

Extracellular electrophysiology.—Electrophysiological signals were acquired with a 32-site polytrode acute probe (A4×8-5mm-100-400-177-A32 (4 shanks at 400 μm spacing, 8 site/shank at 100 μm spacing, NeuroNexus) through an A32-OM32 adaptor connected to a Cereplex digital headstage (Blackrock Microsystems). Unfiltered signals were digitized at 30 kHz at the headstage and recorded by a Cerebus multichannel data acquisition system (Blackrock Microsystems).

On the day of recording, the cranial window (and the optic fiber, if it was already implanted from behavioral experiments) was removed, and a small durotomy performed to allow insertion of the electrode in visual cortex. A ground wire was connected via a gold pin cemented in a burrhole in the anterior portion of the brain. The probe was slowly lowered into the brain (over the course of 15 min with travel length of around 800 μm) until the most superficial recording site was in the brain and allowed to stabilize for 45 - 60 min before beginning recordings. The 4-shank probe was targeted so that one shank was centered on the injection site. In some cases, all four shanks were in V1; in other cases, they might span across V1 and HVAs, or all be in lateral or medial HVAs.

For optogenetic stimulation, the optic fiber was held in place via an articulated arm (Flexbar, SKU: 14830) to allow light delivery (473 nm LED, Thorlabs) to the injection site. While

mice were viewing gray screen (no visual stimuli), constant blue light was delivered with a duration of either 3.5 s or 3.8 s, which was randomly interleaved with control trials with no light delivery. Between each trial, there was a 4 s ITI to match the condition as in the behavioral task. For viral injections, the light was delivered through 400 mm optic fiber (Thorlabs) with the mean light power 0.34±0.1 mW (range: 0.1-1.5 mW). For transgenic VGAT-ChR2 mice, the light was delivered through 50 mm optic fiber (Thorlabs) and a collimator (Edmund Optics) with the mean light power 0.42±0.01 mW (range: 0.4-0.5 mW). The light delivery methods and light power matched those in the behavioral experiments (Figures 2L, 3L and S3).

To measure orientation tuning and responses to task stimuli in V1 and the HVAs (Figure 3C–F), we presented five repetitive static, 100 ms sine-wave gratings with the same orientation (randomized from 0°, 30°, 60°, 90°, 120°, 150°) with an ISI of either 250 or 500 ms and an ITI of 4 s. The contrast of all the stimuli was 100% and spatial frequency was 0.1 cycle/degree, matching those used in the orientation discrimination task. Thus, we used the response to the first stimulus in each trial to measure each neuron's orientation tuning; only trials with an orientation of 0° were used to measure responses to the task distractor stimulus.

Two Photon Imaging.—Calcium imaging data was collected using a microscope controlled by Scanbox software (Neurolabware). Excitation light (920 nm) from a Mai Tai eHP DeepSee laser (Newport) was directed into a modulator (Conoptics) and raster scanned onto the brain with a resonant galvanometer (8 kHz, Cambridge Technology) through a 16X (0.8 NA, Nikon) water-immersion lens. Average power at the surface of the brain was 30-50 mW. Frames were collected at 15 Hz for a FOV of 400×600 pm. Emitted photons were directed through a green filter (510 ± 42 nm band filter; Semrock) onto GaAsP photomultipliers (H10770B-40, Hamamatsu). Images were captured 200 pm below the pia.

During imaging sessions, mice were head restrained while allowed to freely run on a circular disc (InnoWheel, Bio-Serv) and oriented 45° relative to the monitor. To measure neuronal responses to speed increments (Figure 5B–C), we presented random dot kinetograms with the same parameters as were used during the behavioral experiments, in which non-coherently moving dots drifted at 0.5 deg/s for 6 s before incrementing in speed (1.9, 3.8, 7.5, 15 or 30 deg/s) for 3 s, with an ITI of 3 s. On randomly interleaved trials, the contrast of the dots in the baseline condition was set to 0, so that after 6 s the dots appeared at the target speed. Each mouse (n = 6) was imaged for a single session in each area (AL and PM).

QUANTIFICATION AND STATISTICAL ANALYSIS

Behavior processing and analysis.—All behavioral processing and analysis were performed in MATLAB. All trials were categorized as either an early release, hit, or miss based on the time of release relative to target onset: responses occurring earlier than 100 ms after the target stimulus were considered early releases; responses occurring within the reaction window (orientation/contrast task: 200-550 ms; speed task: 200-700 ms) after the target were considered hits; failures to respond before 550 ms (or 700 ms for speed task) after the target were considered misses. For the orientation task, the same reaction window

was used following each distractor to calculate false alarm (FA) rate (FAs are a subset of early releases). Thus, each distractor presentation was categorized as either a FA or correct reject (CR), and each target presentation was either a hit or a miss. Since there were no distractors presented in the contrast and speed increment detection task, we calculated FA rate by simulating the timing of potential distractor presentations to match the distribution of target presentations and assessing the probability of the mouse releasing the lever during these windows.

Behavioral sessions were manually cropped to include stable periods of performance. This typically involved removing trials from the end of the session when motivation had decreased resulting in a high lapse rate (>0.3); we also sometimes removed trials from the beginning of the session that had high early release rate (>0.5) or lapse rates (>0.3) before the mouse began working reliably. Trials were only cropped from the beginning or end of a session, such that each session included at least 200 consecutive trials, and control and suppression trials were interleaved. After cropping, sessions were selected based on the following criteria: 1) at least 40% of trials were hits; and 2) less than 50% of trials were early releases. Based on these criteria, the data in orientation discrimination (Figure 2) included 17 ± 2 (range: 6-48) sessions for each mouse with 5675 ± 596 trials (range: 1982-14851) for contralateral condition; 17 ± 2 (range: 7-36) sessions for each mouse with 5046 ± 698 trials (range: 975-10532) for ipsilateral controls; the data in contrast detection (Figure 4) included 19 ± 2 (range: 5-62) sessions for each mouse with 5938 ± 879 trials (range: 1796-25302) for contralateral condition; 15 ± 2 (range: 4-30) sessions for each mouse with 4291 ± 634 trials (range: 1281-10344) for ipsilateral controls; the data in speed increment detection (Figure 5) included 32±2 sessions (range: 22-44) for each mouse with an average of 7091 ± 795 trials per mouse (range: 5028-13658) for contralateral condition; 20 ± 4 (range: 10-32) sessions for each mouse with 3945 ± 806 trials (range: 1433-6455) for ipsilateral controls.

Hit rate was computed from the number of hits and misses for each stimulus type:

$$Hit\ rate = \frac{hit}{hit + miss}$$

FA rate was computed from the total number of FAs and CRs in the session:

$$FA\ rate = \frac{FA}{FA + CR}$$

Signal detection theory [64] was applied to measure neuronal sensitivity (d'). Extreme values of hit and FA rate (i.e. 0 and 1) were replaced with 0.5/n and (n-0.5)/n, respectively, where n is the number of target or distractor trials[35,65]. d' and c were then calculated as follows:

$$d' = Z(HR) - Z(FAR)\ c = -\frac{Z(HR) + Z(FAR)}{2}$$

where Z is the inverse of the cumulative distribution function of the normal Gaussian distribution; HR is hit rate and FAR is FA rate.

Since threshold varied across mice and not all the mice were tested at exactly the same orientation, contrast, or dot speed, we chose the stimuli values that were near the threshold to summarize d' across animals. Thus, the hit rate for 22.5° orientation, 10% contrast, 2 deg/s dots speed were extrapolated based on a Weibull function fitted from the psychometric curve for each mouse.

For characterizing the dependence of performance across trial length for the orientation discrimination task (Figure S5B–C), we divided trials into four bins (950-1450, 1450-1950, 1950-2450, 2450-8000 ms) and only included mice that had at least 20 trials for each target orientation at each bin to ensure reliable measures. Thus, 5/6, 4/7, 5/7, 5/5 mice were selected for V1, LM, AL and PM respectively.

Electrophysiology processing and analysis.—Individual single units were isolated using the SpyKing CIRCUS package (http://spyking-circus.readthedocs.io/en/latest/). Raw data were first high pass filtered (> 500 Hz) and spikes were detected when a filtered voltage trace crossed threshold (9-13 median absolute deviations computed on each channel). A combination of density-based clustering and template matching algorithms were used to automatically cluster the spikes. The resulting clusters were then inspected and adjusted manually using a MATLAB GUI. Clusters with refractory period violations (< 2 ms, >1% violation) in the auto-correlogram and that were not stable across the whole recording session were discarded from the dataset. Clusters were combined if they met each of three criteria by inspection: 1) similar waveforms; 2) coordinated refractory periods in the cross-correlogram; 3) similar inter-spike interval distribution shape. Since each contact site is at least 100 μm apart, unit position was assigned to the contact site which exerts the biggest waveform.

To quantify effects of inhibition by exciting interneurons, spike times across trials (>30 trials) were first converted to peri-stimulus time histograms (PSTHs, bin size: 100 ms; align to the onset the light delivery, with 2 s baseline period). We used a paired t-test to exclude neurons that were significantly driven by blue light, presumably interneurons, from later analysis. In Figure 1B and 3A, each cell's firing rate was normalized by the firing rate during the baseline (2s window before the light onset). To determine the inhibition efficacy, we measured the normalized suppression as:

$$Norm.\ suppression = \frac{FR_{Base} - FR_{Supp}}{FR_{Base}}$$

where FR_{Supp} is the mean firing rate during the light delivery, FR_{Base} is the mean baseline firing rate. Thus, value of 1 means entirely suppressed; values smaller than 0 suggests excited by light. We then averaged these values across neurons to obtain spatial resolution profiles across cortical depth in the light center (Figure S2C) and cortical distance away from light center (Figures 1C **and** S2D). Note that for both of the suppression methods, the degree of suppression was stable across cortical depth in the light center (viral: p=0.11, n=73

cells; transgenic: p=0.63, n=53 cells; Kruskal-Wallis test across depths, excluding ChR+ cells).

To quantify the percentage of area coverage of suppression, we measured the spatial decay constant as a single exponential fit to the response as a function of tangential distance from the injection center, assuming a homogeneous decay constant across visual cortex for a given optogenetic method (Figure 1, PV/GAD:ChR2 (viral injection); Figure S2, VGAT-ChR2 transgenic mouse line). We then estimated the area of activation within each visual area, and the relative distance between each, using the intrinsic imaging (Figure 1A left and S1B) obtained in response to stimuli with position matched to the behavior tasks (elevation 10°, azimuth 30-40°, but with stimulus size larger than used in the behavior: 40° here versus 30° in the behavior). For each mouse, the active region in each area was fitted with an oval to identify its center and area (Figure 1D). Finally, we approximated the percentage of suppression coverage within and across areas by calculating the fraction of each visual cortical area encompassed by the spatial decay constant centered on each area. We then averaged across mice (n=15) to obtain the inhibition coverage profiles traversing through six visual areas (Figure 1E **and** S2E, values were binned as 0-0.1%, 0.1-2%, 2-50%, 50-98%, 98-100%).

For quantification of optogenetic suppression (Figure 3A–B), we selected cells from the electrode shank centered on the LED light which were not significantly excited and could be clearly assigned to an area. Among 73 non-excited cells (out of 82 total) recorded from mice virally expressing ChR, 29, 6, 17 and 6 cells were in area V1, LM, AL and PM, respectively; among 53 non-excited cells (out of 59 total) recorded from mice transgenically expressing ChR, 25, 11 and 14 cells were in V1, AL and PM, respectively. Thus, a total of n=54, 6, 28 and 20 cells were included for measurement of suppression in V1, LM, AL and PM.

Visually evoked responses of each unit were measured based on average peri-stimulus time histograms (PSTHs, bin size: 20 ms) over repeated presentations (>25 trials) of the same stimulus. To account for the difference in the visual response latency among V1 and HVAs (Figure 3C, [66]), we identified “responsive cells” by first finding the peak response from the average across all trials, then measuring the response on each trial as the average within a 100 ms window centered on the peak response bin, and finally determining significance using a paired t-test comparing trial responses to the baseline response (average response during 0-130 ms window before visual onset) either across all trials or in response to the presented six orientations (alpha value was Bonferroni corrected to account for repeated measures). Response amplitudes were measured by subtracting the firing rate at the time of the visual stimulus onset from the average value during the same 100 ms window centering on the peak response bin for each cell. To determine how well the stimulus orientation information is encoded in each area, we measured circular variance (Figure 3E) [67]:

$$CirVar = 1 - \left| \frac{\sum_k R(\theta_k) \exp(2i\theta_k)}{\sum_k R(\theta_k)} \right|$$

where $R(\theta_k)$ is the response to a sampled orientation θ_k (choosing from 0°, 30°, 60°, 90°, 120°, 150°) and i is the imagery unit. Thus, CirVar has the range from 0 to 1, with value of 0

indicating maximal orientation selectivity and value of 1 indicating lack of orientation selectivity. Signal-to-noise ratio (SNR) in Figure 3F was defined as mean divided by the standard deviation across trials for each cell's preferred orientation.

Two-photon imaging processing and analysis.—All two-photon imaging data was analyzed using custom code written in MATLAB (Mathworks). Image stacks from each imaging session were registered for x-y motion to the same stable reference image selected out of several 500-frame-average images, using Fourier domain subpixel 2D rigid body registration.

Cell bodies were manually segmented from 1) a heatmap generated by determining the temporal correlation of each pixel with its immediate neighbors (where high local correlations yield bright pixels) and 2) the average response during the first second of stimulus presentation (where F is the average of 1 second preceding the stimulus) for each unique target dot stimulus. Together this allowed us to identify most active cells in the field of view (n=6 sessions/area: AL: n = 1692 cells; PM: n = 1396). Fluorescence time courses were generated by averaging all pixels in a cell mask. Neuropil signals were removed by first selecting a shell around each neuron (excluding neighboring neurons), estimating the neuropil scaling factor (by maximizing the skew of the resulting subtraction), and removing this component from each cell's time course. Visually evoked responses were measured as the average dF/F during a window from 200-733 ms after stimulus onset to mimic the reaction window during the behavioral task (the extra 33 ms is due to the limitations of the 15 Hz imaging rate).

Cells were categorized as visually responsive if they had statistically significant responses to at least one stimulus condition (either presentation of dots or increment in speed) compared to a similar baseline window, as measured with a one-sided t-test with the significance threshold Bonferroni corrected for the number of stimulus conditions. Cells were categorized as increment responsive if they had statistically significant responses to at least one speed increment. Cells were categorized as tuned if they passed a one-way ANOVA for responses across speeds. The preferred speed was defined as the speed increment that drove the maximal response for each speed-tuned cell.

Speed response functions were fit with a Naka-Rushton hyperbolic function:

$$R = R_{max}\frac{S^n}{\left(S^n + S_{50}^n\right)}$$

where R is dF/F response, S is stimulus speed, n is exponent of power function (constrained >1), and S_{50} is speed of half-max response. Tuned cells where the model fit with an R^2 greater than 0.5 were considered to be well-fit.

Experimental Design and Statistical Analysis

All behavioral and neuronal data were tested for normality using a Lilliefors test. While behavioral measures were normally distributed, electrophysiological measures of spike rates

were not. Therefore, behavioral data were compared with either a t-test or ANOVA with post hoc Tukey HSD test for datasets with two and multiple groups, respectively. However, for the neuronal activity we used only non-parametric tests (Wilcoxon signed rank test and Friedman test with post hoc Tukey HSD test to compare two and multiple groups, respectively). Sample sizes were not predetermined by statistical methods, but are similar to other studies. The numbers of cells, animals or experiments were provided in the corresponding text, figures and figure legends. All error values in the text are SEMs unless otherwise specified. Data collection and analysis were not performed blind to experimental conditions, but all visual presentation and optogenetic stimulation conditions in behavior and electrophysiology experiments are randomized.

Data and code availability

All relevant data and code are available from the corresponding author upon reasonable request.

Supplementary Material

Refer to Web version on PubMed Central for supplementary material.

Acknowledgements

We thank J. Sims, A. McKinney and B. Gincley for assistance with behavioral training; E. Burke, K. Leonard, M. Fowler, J. Isaac and K. Murgas for surgical assistance; Z. Xu for assistance with software development; G. Field, C. Hull, S. Lisberger, F. Wang and members of the Hull and Glickfeld labs for helpful discussions and comments on the manuscript. This work was supported by an NIH Director's New Innovator Award (DP2-EY025439), the Pew Biomedical Trusts, and the Alfred P. Sloan Foundation (L.L.G).

References

1. Nassi JJ, and Callaway EM (2009). Parallel processing strategies of the primate visual system. Nat. Rev. Neurosci 10, 360–72. [PubMed: 19352403]
2. Stone J, Dreher B, and Leventhal A (1979). Hierarchical and parallel mechanisms in the organization of visual cortex. Brain Res. 180, 345–94. [PubMed: 231475]
3. Kaas JH, and Garraghty PE (1991). Hierarchical, parallel, and serial arrangements of sensory cortical areas: connection patterns and functional aspects. Curr. Opin. Neurobiol 1, 248–251. [PubMed: 1821188]
4. Merigan W, and Maunsell J (1993). How parallel are the primate visual pathways? Annu. Rev. Neurosci 16, 369–402. [PubMed: 8460898]
5. Brewer AA, Press WA, Logothetis NK, and Wandell BA (2002). Visual areas in macaque cortex measured using functional magnetic resonance imaging. J. Neurosci 22, 10416–10426. [PubMed: 12451141]
6. DeYoe EA, Carman GJ, Bandettini P, Glickman S, Wieser J, Cox R, Miller D, and Neitz J (1996). Mapping striate and extrastriate visual areas in human cerebral cortex. Proc. Natl. Acad. Sci. U. S. A 93, 2382–2386. [PubMed: 8637882]
7. Garrett ME, Nauhaus I, Marshel JH, and Callaway EM (2014). Topography and Areal Organization of Mouse Visual Cortex. J. Neurosci 34, 12587–12600. [PubMed: 25209296]
8. Ungerleider LG, and Mishkin M (1982). Two cortical visual systems. In In Analysis of Visual Behavior, Ingle D, Goodale M, and Mansfield R, eds. (Cambridge, MA: MIT Press), pp. 549–586.
9. Goodale MA, and Milner AD (1992). Separate visual pathways for perception and action. Trends Neurosci. 15, 20–5. [PubMed: 1374953]

10. Shipp S, and Zeki S (1985). Segregation of pathways leading from area V2 to areas V4 and V5 of macaque monkey visual cortex. Nature 315, 322–324. [PubMed: 2987702]
11. Schiller P (1993). The effects of V4 and middle temporal (MT) area lesions on visual performance in the rhesus monkey. Vis. Neurosci 10, 717–46. [PubMed: 8338809]
12. Pitcher D, Walsh V, Yovel G, and Duchaine B (2007). TMS Evidence for the Involvement of the Right Occipital Face Area in Early Face Processing. Curr. Biol 17, 1568–1573. [PubMed: 17764942]
13. Lennie P (1998). Single Units and Visual Cortical Organization. Perception 27, 889–935. [PubMed: 10209632]
14. Rentzeperis I, Nikolaev AR, Kiper DC, and van Leeuwen C (2014). Distributed processing of color and form in the visual cortex. Front. Psychol 5, 1–14. [PubMed: 24474945]
15. Konen CS, and Kastner S (2008). Two hierarchically organized neural systems for object information in human visual cortex. Nat. Neurosci 11, 224–231. [PubMed: 18193041]
16. Murgas K, Wilson A, Michael V, and Glickfeld L (2020). Unique spatial integration in mouse primary visual cortex and higher visual areas. J. Neurosci 40, 1862–1873. [PubMed: 31949109]
17. de Vries SEJ, Lecoq JA, Buice MA, Groblewski PA, Ocker GK, Oliver M, Feng D, Cain N, Ledochowitsch P, Millman D, et al. (2020). A large-scale standardized physiological survey reveals functional organization of the mouse visual cortex. Nat. Neurosci 23, 138–151. [PubMed: 31844315]
18. Marshel JH, Garrett ME, Nauhaus I, and Callaway EM (2011). Functional Specialization of Seven Mouse Visual Cortical Areas. Neuron 72, 1040–1054. [PubMed: 22196338]
19. Andermann ML, Kerlin AM, Roumis DK, Glickfeld LL, and Reid RC (2011). Functional specialization of mouse higher visual cortical areas. Neuron 72, 1025–39. [PubMed: 22196337]
20. Wang Q, and Burkhalter A (2007). Area Map of Mouse Visual Cortex. J Comp Neurol. 502, 339–357. [PubMed: 17366604]
21. Kasper EM, Larkman AU, LQbke J, and Blakemore C (1994). Pyramidal neurons in layer 5 of the rat visual cortex. I. Correlation among cell morphology, intrinsic electrophysiological properties, and axon targets. J. Comp. Neurol 339, 459–474. [PubMed: 8144741]
22. Kim EJ, Juavinett AL, Kyubwa EM, Jacobs MW, and Callaway EM (2015). Three Types of Cortical Layer 5 Neurons That Differ in Brain-wide Connectivity and Function. Neuron 88, 1253–1267. [PubMed: 26671462]
23. Tang L, and Higley MJ (2020). Layer 5 Circuits in V1 Differentially Control Visuomotor Behavior. Neuron 105, 346–354.e5. [PubMed: 31757603]
24. D'Souza RD, Meier AM, Bista P, Wang Q, and Burkhalter A (2016). Recruitment of inhibition and excitation across mouse visual cortex depends on the hierarchy of interconnecting areas. Elife 5, e19332. [PubMed: 27669144]
25. Siegle JH, Jia X, Durand S, Gale S, Bennett C, Phillips JW, Reid RC, Mihalas S, Olsen SR, and Koch C (2019). A survey of spiking activity reveals a functional hierarchy of mouse corticothalamic visual areas. bioRxiv, 805010.
26. Licata AM, Kaufman MT, Raposo D, Ryan MB, Sheppard JP, and Churchland AK (2017). Posterior parietal cortex guides visual decisions in rats. J. Neurosci 37, 0105–17.
27. Odoemene O, Pisupati S, Nguyen H, and Churchland AK (2018). Visual Evidence Accumulation Guides Decision-Making in Unrestrained Mice. J. Neurosci 38, 10143–10155. [PubMed: 30322902]
28. Erlich JC, Brunton BW, Duan CA, Hanks TD, and Brody CD (2015). Distinct effects of prefrontal and parietal cortex inactivations on an accumulation of evidence task in the rat. Elife 4, e05457.
29. Lien AD, and Scanziani M (2013). Tuned thalamic excitation is amplified by visual cortical circuits. Nat. Neurosci 16.
30. Glickfeld LL, Histed MH, and Maunsell JHR (2013). Mouse Primary Visual Cortex Is Used to Detect Both Orientation and Contrast Changes. J. Neurosci 33, 19416–22. [PubMed: 24336708]
31. Li N, Chen S, Guo ZV, Chen H, Huo Y, Inagaki HK, Chen G, Davis C, Hansel D, Guo C, et al. (2019). Spatiotemporal constraints on optogenetic inactivation in cortical circuits. Elife 8, e48622. [PubMed: 31736463]

32. Resulaj A, Ruediger S, Olsen SR, and Scanziani M (2018). First spikes in visual cortex enable perceptual discrimination. Elife 7, e34044. [PubMed: 29659352]
33. Jin M, and Glickfeld LL (2019). Contribution of Sensory Encoding to Measured Bias. J. Neurosci 39, 5115–5127. [PubMed: 31015339]
34. Jin M, Beck JM, and Glickfeld LL (2019). Neuronal adaptation reveals a suboptimal decoding of orientation tuned populations in the mouse visual cortex. J. Neurosci 39, 3172–18. [PubMed: 31019047]
35. Macmillan NA, and Kaplan HL (1985). Detection theory analysis of group data: Estimating sensitivity from average hit and false-alarm rates. Psychol. Bull 98, 185–199. [PubMed: 4034817]
36. Histed MH, Carvalho LA, and Maunsell JHR (2012). Psychophysical measurement of contrast sensitivity in the behaving mouse. J. Neurophysiol 107, 758–765. [PubMed: 22049334]
37. Roth MM, Helmchen F, and Kampa BM (2012). Distinct Functional Properties of Primary and Posteromedial Visual Area of Mouse Neocortex. J. Neurosci 32, 9716–9726. [PubMed: 22787057]
38. Murakami T, Matsui T, and Ohki K (2017). Functional Segregation and Development of Mouse Higher Visual Areas. J. Neurosci, 0731–17.
39. Han X, Vermaercke B, and Bonin V (2018). Segregated encoding of spatiotemporal features in the mouse visual cortex. bioRxiv, 441014.
40. Yu Y, Stirman JN, Dorsett CR, and Smith SL (2019). Mesoscale correlation structure with single cell resolution during visual coding. bioRxiv, 469114.
41. Zhao X, Liu M, and Cang J (2014). Visual Cortex Modulates the Magnitude but Not the Selectivity of Looming-Evoked Responses in the Superior Colliculus of Awake Mice. Neuron, 1–12.
42. Otchy TM, Wolff SBE, Rhee JY, Pehlevan C, Kawai R, Kempf A, Gobes SMH, and Olveczky BP (2015). Acute off-target effects of neural circuit manipulations. Nature 528, 358–363. [PubMed: 26649821]
43. Wang Q, Gao E, and Burkhalter A (2011). Gateways of Ventral and Dorsal Streams in Mouse Visual Cortex. J. Neurosci 31, 1905–1918. [PubMed: 21289200]
44. Pafundo DE, Nicholas MA, Zhang R, and Kuhlman SJ (2016). Top-Down-Mediated Facilitation in the Visual Cortex Is Gated by Subcortical Neuromodulation. J. Neurosci 36, 2904–2914. [PubMed: 26961946]
45. Keller AJ, Roth MM, and Scanziani M (2020). Feedback generates a second receptive field in neurons of the visual cortex. Nature 582, 545–549. [PubMed: 32499655]
46. Vangeneugden J, van Beest EH, Cohen MX, Lorteije JAM, Mukherjee S, Kirchberger L, Montijn JS, Thamizharasu P, Camillo D, Levelt CN, et al. (2019). Activity in Lateral Visual Areas Contributes to Surround Suppression in Awake Mouse V1. Curr. Biol 29, 4268–4275.e7. [PubMed: 31786063]
47. Wang Q, and Burkhalter A (2013). Stream-related preferences of inputs to the superior colliculus from areas of dorsal and ventral streams of mouse visual cortex. J. Neurosci 33, 1696–705. [PubMed: 23345242]
48. Wang L, Rangarajan KV, Gerfen CR, and Krauzlis RJ (2018). Activation of Striatal Neurons Causes a Perceptual Decision Bias during Visual Change Detection in Mice. Neuron 97, 1369–1381.e5. [PubMed: 29503185]
49. Fehervari TD, and Yagi T (2016). Population Response Propagation to Extrastriate Areas Evoked by Intracortical Electrical Stimulation in. Front Neural Circuits 10, 1–14. [PubMed: 26834567]
50. Coogan TA, and Burkhalter A (1993). Hierarchical organization of areas in rat visual cortex. J. Neurosci 13, 3749–72. [PubMed: 7690066]
51. Esfahany K, Siergiej I, Zhao Y, and Park IM (2018). Organization of Neural Population Code in Mouse Visual System. 5, 1–10.
52. Cai L, Wu B, and Ji S (2018). Neuronal Activities in the Mouse Visual Cortex Predict Patterns of Sensory Stimuli. Neuroinformatics 16, 473–488. [PubMed: 29404932]
53. Tsunada J, Liu ASK, Gold JI, and Cohen YE (2015). Causal contribution of primate auditory cortex to auditory perceptual decision-making. Nat. Neurosci 19, 135–142. [PubMed: 26656644]
54. Katz LN, Yates JL, Pillow JW, and Huk AC (2016). Dissociated functional significance of decision-related activity in the primate dorsal stream. Nature 535, 285–288. [PubMed: 27376476]

55. Liu LD, and Pack CC (2017). The Contribution of Area MT to Visual Motion Perception Depends on Training. Neuron 95, 436–446.e3. [PubMed: 28689980]
56. Zatka-Haas P, Steinmetz NA, Carandini M, and Harris KD (2019). Distinct contributions of mouse cortical areas to visual discrimination. bioRxiv, 501627.
57. Bennett C, Gale SD, Garrett ME, Newton ML, Callaway EM, Murphy GJ, and Olsen SR (2019). Higher-Order Thalamic Circuits Channel Parallel Streams of Visual Information in Mice. Neuron 102, 477–492.e5. [PubMed: 30850257]
58. Wang Q, Sporns O, and Burkhalter A (2012). Network Analysis of Corticocortical Connections Reveals Ventral and Dorsal Processing Streams in Mouse Visual Cortex. J. Neurosci 32, 4386–4399. [PubMed: 22457489]
59. Nassi JJ, Lomber SG, and Born RT (2013). Corticocortical feedback contributes to surround suppression in V1 of the alert primate. J. Neurosci 33, 8504–17. [PubMed: 23658187]
60. Nurminen L, Merlin S, Bijanzadeh M, Federer F, and Angelucci A (2018). Top-down feedback controls spatial summation and response amplitude in primate visual cortex. Nat. Commun 9, 2281. [PubMed: 29892057]
61. Fang Q, Chou X, Peng B, Zhong W, Zhang LI, and Tao HW (2020). A Differential Circuit via Retino-Colliculo-Pulvinar Pathway Enhances Feature Selectivity in Visual Cortex through Surround Suppression. Neuron 105, 355–369.e6. [PubMed: 31812514]
62. Znamenskiy P, and Zador AM (2013). Corticostriatal neurons in auditory cortex drive decisions during auditory discrimination. Nature 497, 482–5. [PubMed: 23636333]
63. Goldey GJ, Roumis DK, Glickfeld LL, Kerlin AM, Reid RC, Bonin V, Schafer DP, and Andermann ML (2014). Removable cranial windows for longterm imaging in awake mice. Nat. Protoc 9, 2515–2538. [PubMed: 25275789]
64. Green DM, and Swets J (1966). Signal detection theory and psychophysics (Wiley).
65. Stanislaw H, and Todorov N (1999). Calculation of signal detection theory measures. Behav. Res. Methods Instrum. Comput 31, 137–149. [PubMed: 10495845]
66. Jin M, and Glickfeld LL (2020). Magnitude, time course, and specificity of rapid adaptation across mouse visual areas. J. Neurophysiol 124, 245–258. [PubMed: 32584636]
67. Mazurek M, Kager M, and Van Hooser SD (2014). Robust quantification of orientation selectivity and direction selectivity. Front. Neural Circuits 8, 92. [PubMed: 25147504]

Highlights:

- Suppressing LM and AL impairs orientation discrimination and contrast detection
- This suggests that higher-order areas are needed in perception of simple features
- PM encodes task-relevant signals, but suppressing PM has no effect on threshold
- Yet, suppressing PM increases FA rates on some tasks, suggesting a non-visual role

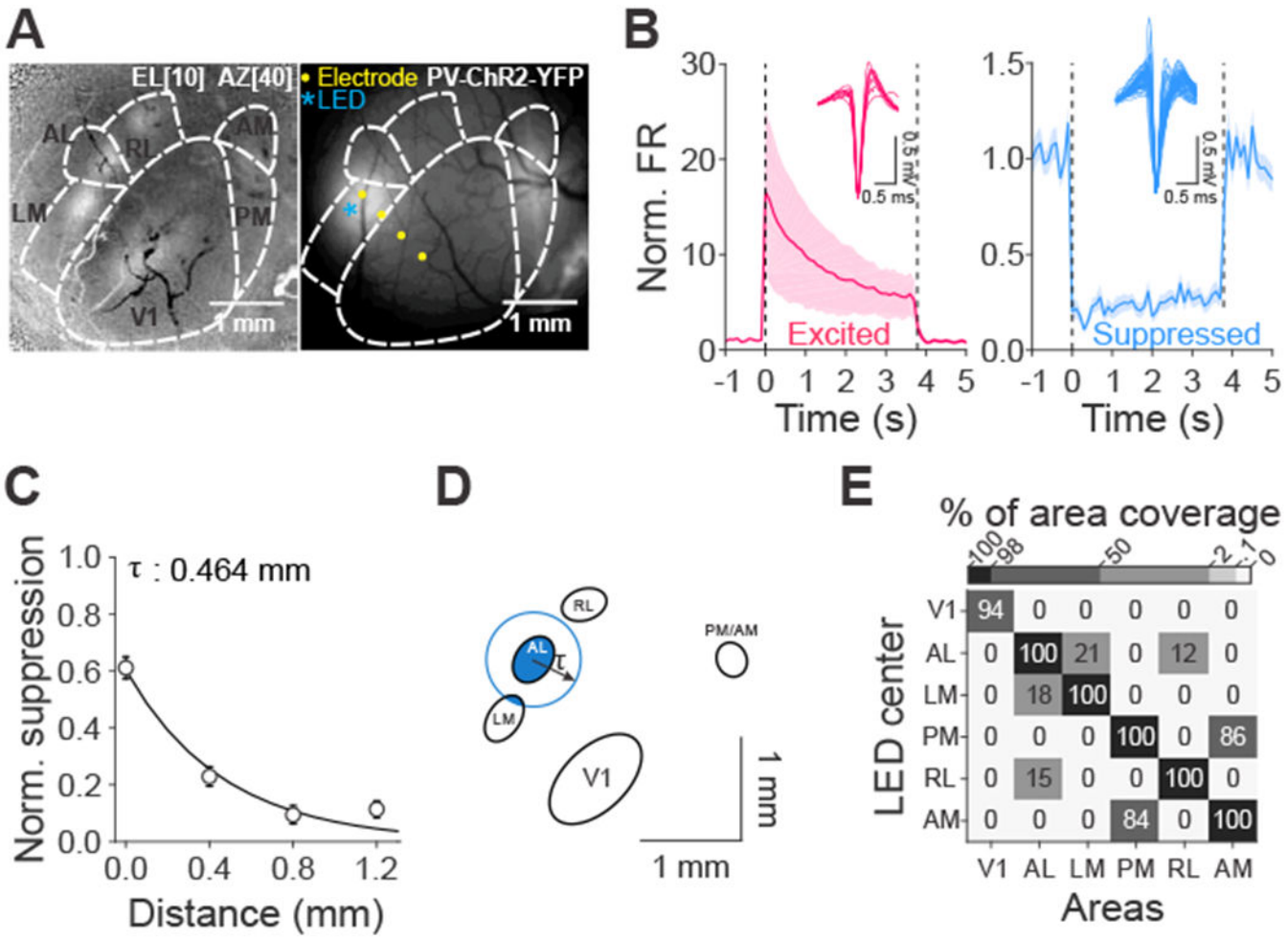

Figure 1 –. Efficacy and spatial resolution of optogenetic inhibition of mouse visual areas.

(**A**) Left: change in intrinsic autofluorescence in response to a visual stimulus at elevation 10°, azimuth 40°, size 40°. Increases in fluorescence reflect activation. Right: viral expression of ChR2 in parvalbumin positive (PV+) interneurons in LM and PM. (**B**) Normalized spontaneous firing rates (FR) of cells that are excited (left, red, n=9 cells) and suppressed (right, blue, n=58 cells) when stimulated with 473 nm LED light. Dashed lines indicate light onset and offset. Insets are the waveforms of single units. ChR2 is expressed in either PV+ or GAD+ interneurons. Light power: 0.1-1.5 mW across 16 experiments (n=12 mice). (**C**) Normalized suppression as a function of distance from the LED center (0 mm). Error bars are SEM across cells (n=73, 97, 81, 50 cells from 0 to 1.2 mm). The decay constant (**τ**) was calculated via a single exponential fit. (**D**) Oval fits for visual areas for the same example mouse in **A** with a demonstration of calculating percentage of area coverage when light is centered on AL. Blue circle was drawn based on the radius of **τ** from the fit in **C**. (**E**) Mean percentage of area coverage of inhibition across mice (n=15 mice). See also Figures S1 and S2.

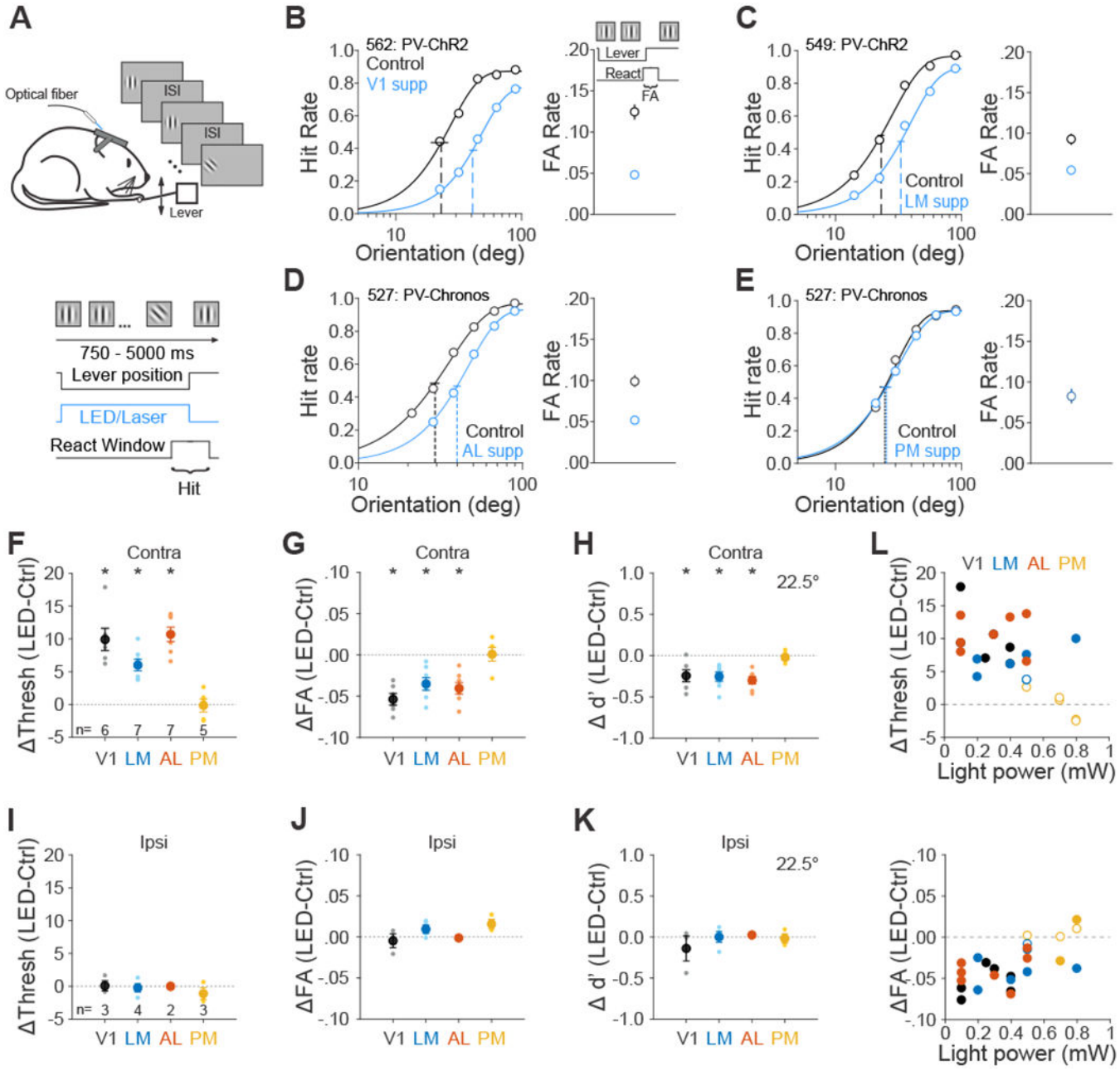

Figure 2 –. Role of mouse visual areas in an orientation discrimination task.

(**A**)chematic of orientation discrimination task. (**B-E**) Effect of suppression in area V1 (**B**), LM (**C**), AL (**D**), and PM (**E**) on the task performance for each representative mouse. Note that data from AL and PM come from the same mouse. Left- hit rate (Hit/(Hit + Miss)) as a function of target orientations. Data were fitted by Weibull functions to determine the thresholds (dotted vertical lines) and 95% confidence intervals (solid horizontal lines). Right- false alarm (FA) rate calculated as FA/(FA + CR). CR: correct rejection. Supp: suppression. Error bars are 95% confidence intervals. (**F-I**) Summary of effect of suppression in visual areas in terms of the change in the threshold (**F**), FA rate (**G**) and sensitivity (d' for 22.5° target, **H**). Big circles are the population mean and small circles are

data for each mouse. The visual stimulus is presented in the contralateral field of view (relative to the ChR2 injection site). Error bars indicate ± SEM across mice (n=6, 7, 7, 5 for V1, LM, AL, and PM respectively). * $p<0.05$. (**I-K**) Same as **F-H**, for visual stimulus presentation in the ipsilateral field of view. n=3, 4, 2, 3 for V1, LM, AL and PM respectively. (L) Effects of area suppression on orientation discrimination threshold (top) and FA rate (bottom) as a function of light power. Different colors denote different visual areas. Filled and open circles denote significant and non-significant difference between control and suppression trials, respectively. See also Figures S3, S4 and S5 and Data S1 and S2.

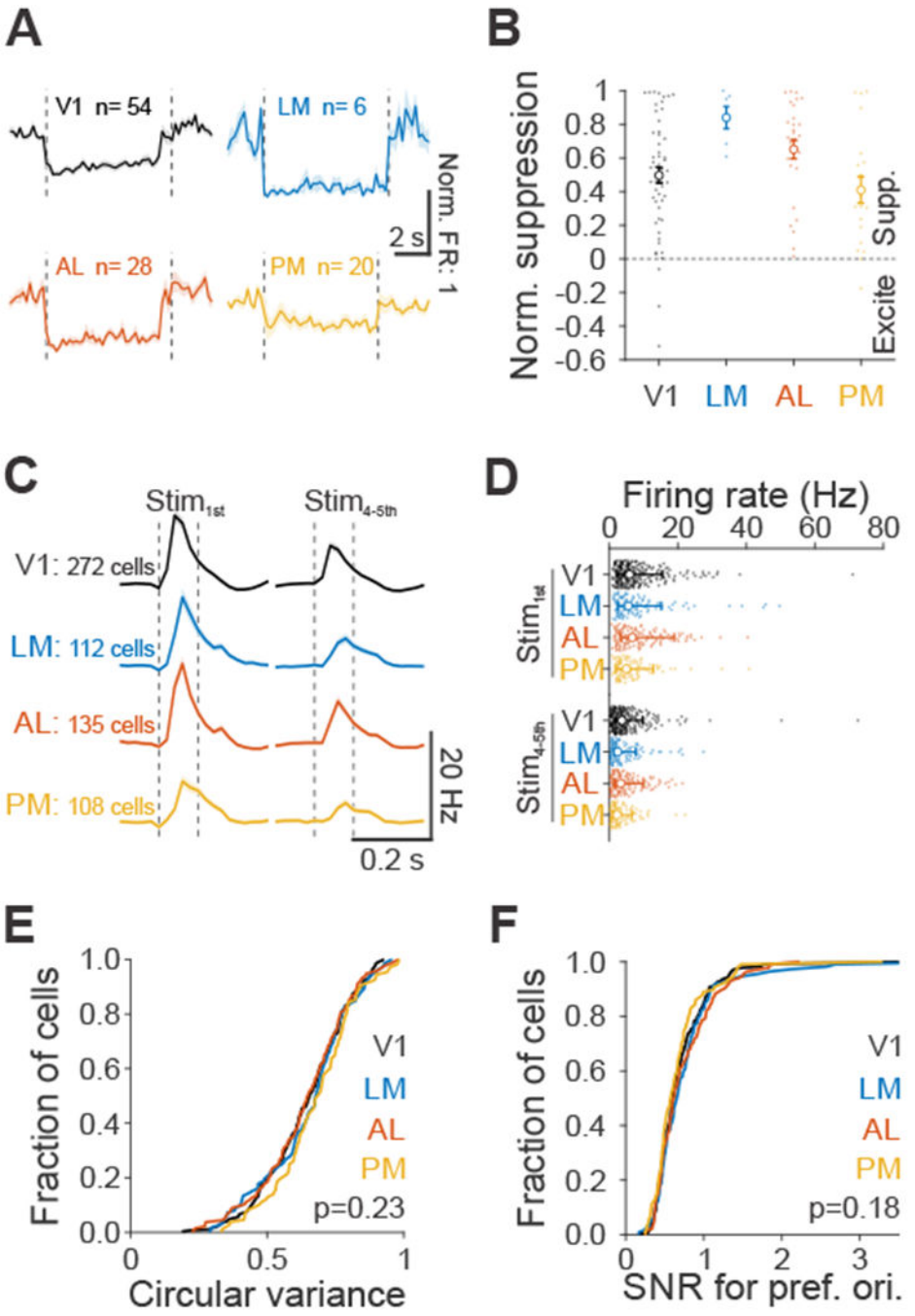

Figure 3 –. Comparison of suppression efficacy and visually driven response properties across mouse visual areas.

(**A**) Average spontaneous firing rates (FR), normalized to baseline FR, during ChR activation with blue light for each area. Dashed vertical lines indicate light onset and offset. Cells that were excited were removed and recordings from viral (V; Figure 1) and transgenic (T; Figure S2) approaches were combined (V1: n= V:29, T:25; LM: n= V:6, T:0; AL: n= V:17, T:11; PM: n= V:6, T:14). Shaded error is SEM across cells. (**B**) Normalized suppression across areas, summarized from **A**. Small filled dots are individual cells, open

circles are means across population and error bars are SEM across cells. (**C**) Grand average of neuronal response to first (left, $Stim_{1st}$) and plateaued fourth and fifth stimuli (right, $Stim_{4\text{-}5th}$) at its preferred orientation for visually responsive cells (V1: n=272; LM: n=112; AL: n=135; PM: n=108 cells). Dashed vertical lines indicate visual stimulus onset and offset. Shaded error is SEM across cells. (**D**) Summary of neuronal response to $Stim_{1st}$ (top) and $Stim_{4\text{-}5th}$ (bottom) for cells in **C**. Each small filled dot is a single cell, open circle is the median of the population and error bars are 25th and 75th percentile. (**E**) Cumulative distribution of the circular variance responses across orientations, for each area. Same cells as in **C**. (**F**) Same as **E**, for signal-to-noise ratio (SNR, mean/std) at the preferred orientation for each cell.

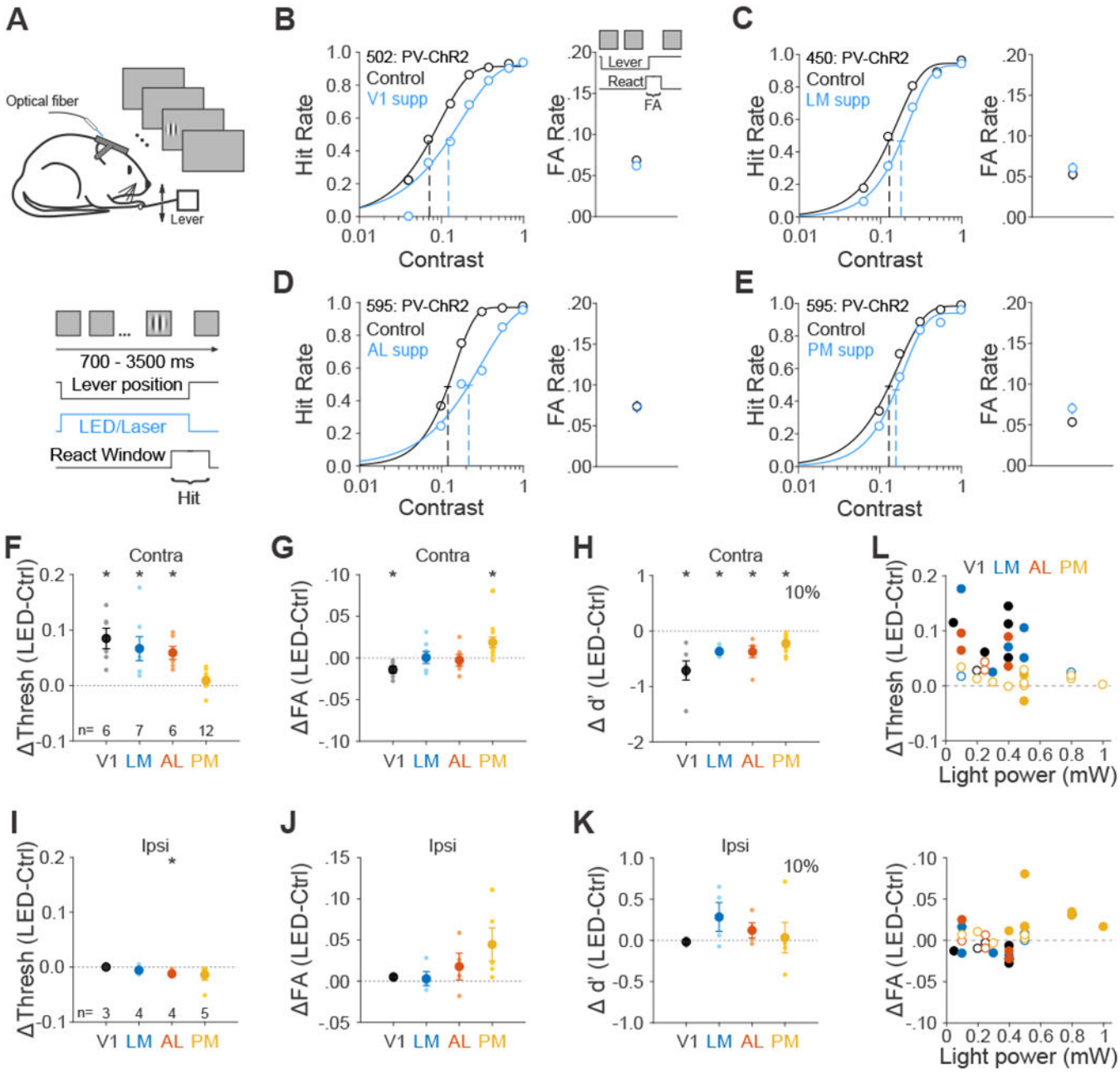

Figure 4 –. Role of mouse visual areas in detecting stimulus contrast.

(**A**) Schematic of contrast detection task. (**B-E**) Effect of suppression in area V1 (B), LM (**C**), AL (**D**) and PM (**E**) on performance for each representative mouse. Note that data from AL and PM come from the same mouse. Left- hit rate as a function of stimulus contrast. Data were fitted by Weibull functions to determine the thresholds (dotted vertical lines) and 95% confidence intervals (solid horizontal lines). Right- FA rate. Error bars are 95% confidence intervals. (**F-H**) Summary of effect of suppression in visual areas in terms of the change in the threshold (**F**), FA rate (**G**) and sensitivity (d' for 10% contrast, **H**). Big circles are the population mean and small circles are data for each mouse. The visual stimulus is presented in the contralateral field of view (relative to the ChR2 injection site). Error bars

indicate ± SEM across mice (n=6, 7, 6, 12 for V1, LM, AL, and PM respectively). * $p<0.05$. (**I-K**) Same as **F-H**, for visual stimulus presentation in the ipsilateral field of view. n=3, 4, 4, 5 for V1, LM, AL and PM respectively. (**L**) Effects of area suppression on contrast detection threshold (top) and FA rate (bottom) as a function of light power. Different colors denote different visual areas. Filled and open circles denote significant and non-significant difference between control and suppression trials, respectively. See also Figures S3 and S4 and Data S3 and S4.

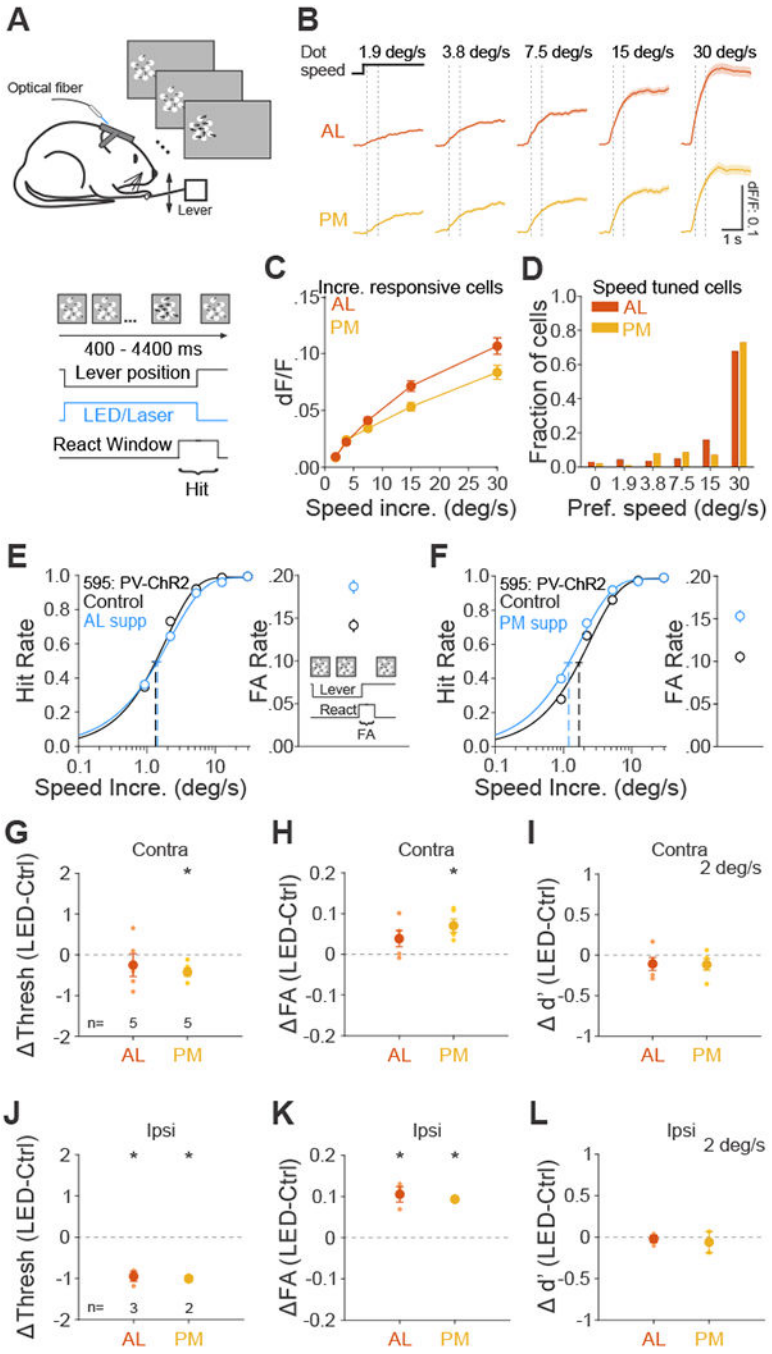

Figure 5 –. Role of areas AL and PM in detecting speed increment.

(**A**) Schematic of speed increment detection task. Base dot speed: 0.5 deg/s, dot coherence: 0%. Thicker arrows indicate an increase in dot speed. (**B**) Grand average of change in fluorescence (dF/F) in response to each speed increment for all cells significantly responsive to speed increments in area AL (top, n=669 cells) and PM (bottom, n=516). Black step horizontal lines show the onset and duration of the speed increment from the base dot speed. Dotted vertical lines show the window for calculating response for each cell in **C** (200-733 ms after onset). (**C**) Summary of neuronal responses of same cells in **B** to each speed

increment. Error is SEM across cells. (**D**) Summary of the fraction of speed tuned cells that prefer each speed increment (AL: n=337 cells; PM: n=169). (**E-F**) Effect of suppression in area AL (**E**) and PM (**F**) on hit rate (left) and FA rate (right) for an example mouse. Note that this is the same mouse from Figure 4D–E. (**G-I**) Summary of effect of suppression in AL and PM in terms of the change in the threshold (**G**), FA rate (**H**) and sensitivity (d' for 2 deg/s speed increment, **I**). Big circles are the population mean and small circles are data for each mouse. The visual stimulus is presented in the contralateral field of view (relative to the ChR2 injection site). Error bars indicate ± SEM across mice (n=5, 5 for AL and PM). * $p<0.05$. (**J-L**) Same as **G-I**, for visual stimulus presentation in the ipsilateral field of view. n=3, 2 for AL and PM. See also Figure S4 and Data S5.

Table 1.
Light power (mW) used for each experiment for three visual tasks.

Summary of tasks performed, areas suppressed, and light powers used for each mouse.

		Visual tasks									
		Orientation discrimination				Contrast detection				Speed	
		V1	LM	AL	PM	V1	LM	AL	PM	AL	PM
Mouse ID and light power (mW)	562	0.1									
	568	0.1				0.05					
	569	0.25									
	536	0.4	0.4	0.4		0.4	0.4	0.4	0.4		
	570	0.3									
	571	0.4	0.2								
	449		0.5		0.8				0.5		
	450		0.5		0.5		0.5				
	512		0.2				0.1				
	549		0.8		0.8						
	543		0.5				0.5		1.0		
	511			0.1				0.1			
	521			0.5					0.5		
	522			0.5							
	527			0.3	0.7						
	544			0.1							
	557			0.1							
	515				0.7				0.5		
	440					0.2			0.2		
	502					0.4					
	503					0.25					
	584					0.4	0.3	0.4	0.3		
	454						0.8		0.5		
	558						0.1		0.8		
	430							0.25			
	438							0.25	0.8	0.5	0.8
	595							0.1	0.5	0.5	0.5
	563								0.1		
	418									0.5	0.5
	423									0.5	0.5
	455									0.5	0.5
n=	31	6	7	7	5	6	7	6	12	5	5